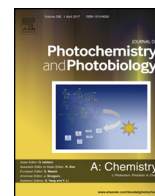




Contents lists available at ScienceDirect

Journal of Photochemistry and Photobiology A: Chemistry

journal homepage: www.elsevier.com/locate/jphotochem

Hollow microspheres consisting of uniform $Zn_xCd_{1-x}S$ nanoparticles with noble-metal-free co-catalysts for hydrogen evolution with high quantum efficiency under visible light

Mohammad Reza Gholipour^a, Chinh Chien Nguyen^a, Francois Béland^b, Trong-On Do^{a,*}

^a Department of Chemical Engineering, Laval University, Québec, G1 V 0A8, Canada

^b SiliCycle Inc. 2500, Boul. du Parc-Technologique, Québec, G1P 4S6, Canada

ARTICLE INFO

Article history:

Received 7 December 2017

Received in revised form 24 January 2018

Accepted 28 February 2018

Available online xxx

Keywords:

Zinc cadmium sulfide

Solid solution

Hydrogen production

Water splitting

Visible light photocatalyst

Solar energy

Noble-metal free cocatalyst

ABSTRACT

Utilizing solar energy in order to produce hydrogen from water is one of the key technologies to deal with energy and environment issues. A photocatalyst with a small band gap, good charge separation, and high stability plays an important role in this process. Recently, zinc cadmium sulfide ($Zn_xCd_{1-x}S$) has caught researchers' attention due to its unique photocatalytic properties such as the wide range of visible light energy absorption and strong stability during water splitting. Moreover, a unique feature of this semiconductor is the capability of modifying its band gap structure by changing the Zn/Cd ratio. Herein, a series of $Zn_xCd_{1-x}S$ solid solutions was synthesized by utilizing metal-glycerate followed by calcination in air and sulfuration under flowing H_2S . As a result, a homogeneous hexagonal wurtzite $Zn_xCd_{1-x}S$ solid solution could produce hydrogen in a wide range of visible light region. Moreover, using MoS_2 as a cocatalyst resulted in the same amount of hydrogen as Pt. The best result was obtained for the $Zn_{30}Cd_{70}S$ solid solution that showed a hydrogen evolution of $12 \text{ mmol h}^{-1} \text{ g}^{-1}$ under solar simulator. The calculated quantum efficiencies (QE) in visible light region are: 46.6% at 400 nm to 23.4% at 500 nm as well as 11.3% at 550 nm. There are among the highest QE that have been ever reported for this kind of material under visible light region.

© 2018 Published by Elsevier B.V.

1. Introduction

No one can deny that the climate changes are happening due to global warming effects of greenhouse gases. One of the main reason for this crucial issue is the use of an immense amount of fossil fuels resulting in the massive emission of carbon dioxide into the atmosphere. One of the promising solutions for this problem is converting solar energy into hydrogen molecules via the photocatalytic process of water splitting. Honda and Fujishima were pioneers of splitting water into hydrogen and oxygen using TiO_2 under UV light [1]. However, the low efficiency of hydrogen production, which originates from absorption limited to the UV region, resulting in a limitation on its practical applications. This motivated many scientists to explore other efficient photocatalysts that can absorb the energy of visible light, which accounts for about 50% of sunlight energy [2–4].

It has been established that CdS can act as a photocatalyst in hydrogen production reaction from water under visible light irradiation because of its narrow band gap and a proper conduction band position [5,6]. The valence band of this metal sulfide is composed by S 3p orbitals located at higher energy levels, resulting in a narrow band gap with a strong visible light response [7,8]. Nonetheless, its high photo-corrosion considerably affects its stability during photocatalysis reactions [9]. As a result, various approaches have been investigated in order to improve its photocatalytic performance [4,10,11]. Among all strategies, making a solid solution with other semiconductors is an interesting method to improve the photoactivity of CdS because of the ability to control conduction and valence bands positions [12].

Zinc Cadmium sulfide solid solutions ($Zn_xCd_{1-x}S$) possess an adjustable band gap width and a good resistance towards photo-corrosion.[13,14] Moreover, they can produce hydrogen more efficiently than CdS [12]. Therefore, researchers have tried different techniques to enhance $Zn_xCd_{1-x}S$ photocatalytic activities [4,5,15–17]. Xing et al. synthesized $Zn_xCd_{1-x}S$ solid solution via a co-precipitation step followed by thermal treatment [18]. They found that its band gap could be varied between 2.2 eV and 3.1 eV

* Corresponding author.

E-mail address: Trong-On.Do@gch.ulaval.ca (T.-O. Do).

based on the value of x and the best hydrogen evolution was found with $x = 0.2$ that led to having a band gap of 2.35 eV. Another group used thermal sulfuration method to enhance the photoactivity of $Zn_xCd_{1-x}S$ solid solution for hydrogen evolution [19]. Doping with other elements or synthesizing nanoparticles of $Zn_xCd_{1-x}S$ solid solution have been used to improve the photocatalytic efficiency under visible light region [20–23]. It should be mentioned that even the different crystal structures of $Zn_xCd_{1-x}S$ could affect its hydrogen evolution performance. For instance, a hexagonal wurtzite crystal structure and cubic zinc-blend phase of this solid solution had various photocatalytic activities [7,24–26]. According to the literature, a photocatalyst with cubic zinc-blend structure showed significantly higher hydrogen production in comparison with hexagonal phase [6,12,25]. Shen et al. showed that even the different synthesis methods of the same solid solution ($Zn_{0.5}Cd_{0.5}S$) could significantly impact the hydrogen production under visible light illumination [27]. Interestingly, Liu et al. reported that $Zn_xCd_{1-x}S$ with nano-twinning structures could prevent the recombination of photoexcited carriers, resulting in considerably higher hydrogen evolution under visible light illumination [28]. Based on their observation, a photocatalyst with Pt as a cocatalyst could generate 1.79 mmol of hydrogen with a QE of 43% at 425 nm. It is proved that defects in the structure of $Zn_xCd_{1-x}S$, could act as electron pools and so promote hydrogen production during photocatalytic water splitting [24]. However, the defect states in semiconductors should be controlled in order to obtain the maximum hydrogen evolution.

In this study, a series of $Zn_xCd_{1-x}S$ solid solutions was synthesized by following metal-glycerate of cadmium and zinc that were later converted to mixed oxides. The fact that the mixture consisted of two metal oxides which were homogeneously mixed together at atomic scale, made the mixture a good precursor for synthesizing a solid solution. This aim was achieved by further sulfuration by reacting with H_2S gas at high temperature. As a result, a highly activated solid solution of $Zn_xCd_{1-x}S$ was obtained that was surprisingly active under a large range of visible light illumination with a high quantum efficiency. This is one further step towards industrial applications of this kind of photocatalysts. Moreover, depositing MoS_2 as a cocatalyst on the surface of this photocatalyst could allow producing as much hydrogen as Pt. Although Pt is one of the most efficient cocatalysts for hydrogen production, its high cost and scarcity put some limitations on its usage in large-scale applications. Replacing Pt with MoS_2 would lead to have a noble-metal free photocatalyst with high quantum efficiency in visible light region.

2. Experimental section

2.1. Sample preparation

Zinc Cadmium sulfide solid solutions were synthesized as follows: First, glycerol and zinc nitrate and cadmium nitrate were dissolved in isopropanol and transferred into an autoclave. The autoclave was heated up to 180 °C for 6 h. During solvothermal treatment, microspheres of carbons were made from glycerol [29]. The microspheres contained numerous $-OH^-$ ions that provided a good capacity to absorb various cations specially Zn^{2+} and Cd^{2+} [30]. Later, the microspheres with adsorbed cations were collected via centrifugation and dried at 70 °C overnight. The obtained samples were calcined at 500 °C for 4 h yielding zinc and cadmium mixed oxide. Subsequently, the mixed oxide was exposed to a flowing gas mixture of H_2S (10%)/Ar at 450 °C for 2 h. Therefore, sulfide (S^{2-}) ions could substitute with oxygen and so the mixed oxide was converted to a mixed sulfide. Different atomic Cd/Zn ratios were used to synthesize of various compositions solid solutions which are noted as $Zn_xCd_{1-x}S$.

2.2. Characterization

TEM images of the samples were obtained using a JEOL JEM 1230 instrument operated at 120 kV. High-resolution TEM (HR-TEM) images were obtained by using JEOL JEM-2100F instrument operated at 300 kV. SEM images were obtained on a JEOL 6360 instrument operated at 15 kV. Powder XRD patterns were obtained on a Bruker SMART APEXII X-ray diffractometer equipped with a Cu K α radiation source ($\lambda = 1.5418 \text{ \AA}$). XPS measurements were carried out in an ion-pumped chamber (evacuated to 10–9 Torr) of a photoelectron spectrometer (Kratos Axis-Ultra) equipped with a focused X-ray source (Al K α , $h\nu = 1486.6 \text{ eV}$). The UV–vis spectra were recorded on a Cary 300 Bio UV–vis spectrophotometer.

2.3. Photocatalytic test

The certain amount of photocatalysts (the optimum amount was 50 mg) was added to 100 ml of an aqueous solution of 0.5 M Na_2S and Na_2SO_3 as a sacrificial reagent. The mixture was purged with nitrogen for 30 min in order to remove dissolved oxygen. Then, it was illuminated under a solar simulator light for 2 h (1:5 AM(ABET), equipped with 150 W Xe lamp) to deposit co-catalyst via photo-deposition technique. After that, the cell was purged again with nitrogen and prepare for hydrogen production test under the same light illumination source with a UV-cut off filter ($\geq 420 \text{ nm}$). A 0.5 ml of gas was sampled intermittently through the septum, and hydrogen was analyzed by gas chromatography equipped with TCD detector and carboxen-1010 capillary column.

The quantum yield (QE) was measured according to follow equations under the same photocatalytic reaction conditions [31]. The photon flux was measured with Newport's power meter (1918-C Optical Power Meter) equipped with a thermopile optical detector.

$$\text{Quantum Efficiency (QE)} = \frac{\text{Number of reacted electrons}}{\text{Number of incident photons}} \times 100$$

$$QE = \frac{2 \times \text{Number of evolved hydrogen molecules}}{\text{Number of incident photons}}$$

3. Results and discussions

3.1. Material characterizations

Fig. 1 exhibits X-ray diffraction (XRD) patterns of the mixed oxide (calcination in air) and solid solution samples (H_2S treatment). Clearly, the mixed oxide consisted of two separate phases of CdO and ZnO. According to the references, ZnO has a hexagonal crystal structure, whereas CdO crystal structure is a cubic. After H_2S treatment, oxygen was replaced by sulfur and thus solid solutions of $Zn_xCd_{1-x}S$ were obtained (Fig. 1B). The XRD peaks of $Zn_{0.9}Cd_{0.1}S$ were very close to index peaks of hexagonal wurtzite phase of ZnS (JCPDS No. 00-003-1093) [24]. It seems that in this concentration, cadmium cations were incorporated into the hexagonal structure of ZnS and simultaneously oxygen atoms were replaced by sulfur atoms. Obviously, the diffraction peaks shifted toward the lower angle because of the enhancement in fringe lattice distance of the ZnS crystal structure due to the larger radius of Cd^{2+} than Zn^{2+} (0.97 and 0.74 Å, respectively). By further increase in Cd content, the peaks shifted to even lower angle and its crystal structure transferred from hexagonal ZnS to hexagonal wurtzite CdS (JCPDS No. 00-041-1049).

The mixed oxide obtained after calcination in air, didn't have a clear band gap structure in visible light region and so it cannot generate excited charge carriers (Fig. 2A). Nevertheless, all solid

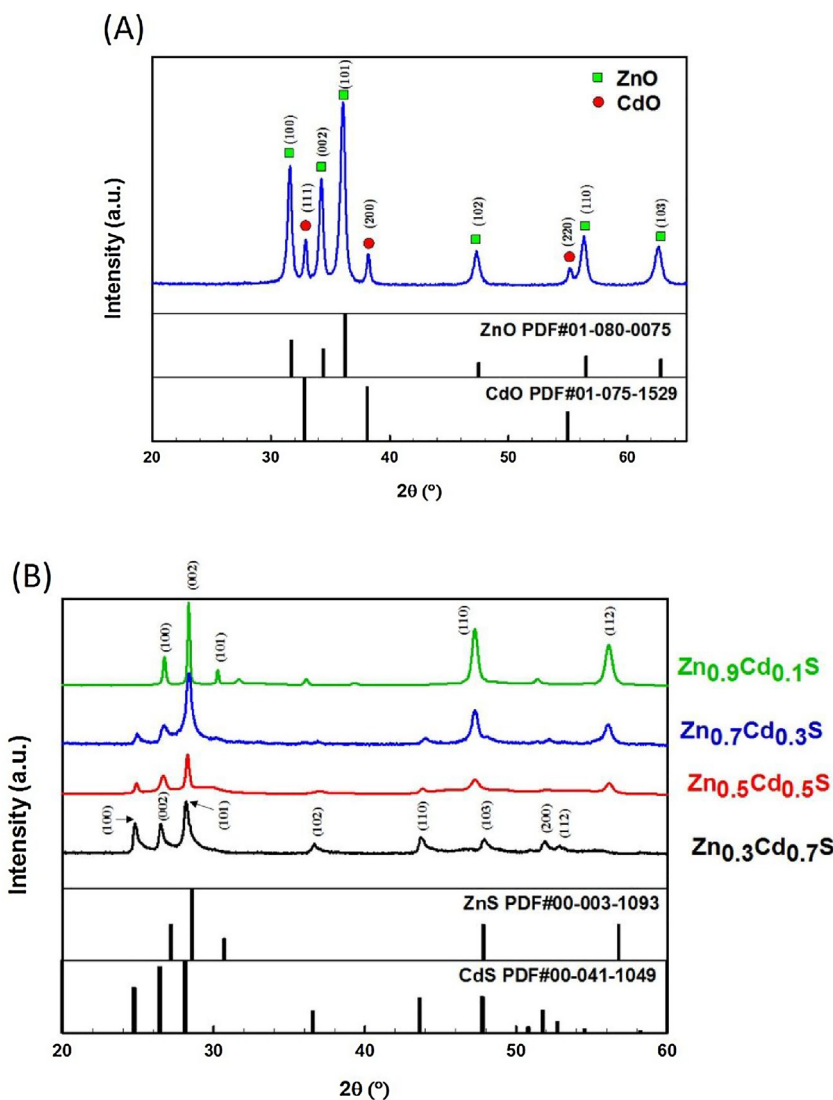


Fig. 1. XRD patterns of (A) $\text{Zn}_{0.5}\text{Cd}_{0.5}\text{O}$ mixed oxide after calcination in air (B) solid solutions of $\text{Zn}_x\text{Cd}_{1-x}\text{S}$ after H_2S treatment.

solutions of $\text{Zn}_{1-x}\text{Cd}_x\text{S}$ exhibited clear band gap structure that can be excited in the visible region. It should be mentioned that ZnS can only be activated under UV light illumination because of its large band gap (3.4 eV). However, by increasing the ratio of Cd, the band gap decreases relatively and so the solid solutions could absorb more visible light energy. The lowest bandgap energy was related to pristine CdS with 2.37 eV as it can be seen in Fig. 2B.

During the solvothermal step, metal-glycerate microspheres (ZnCd -glycerate) were formed in the autoclaves with a help of glycerol and metal cations [29,30]. These microspheres were uniform with an average diameter of 500 nm, as shown in Fig. 3. It should be mentioned that various ratio of Zn and Cd didn't affect the morphology of the microspheres in this step. The metal-glycerate spheres were easily reacted with oxygen in air during calcination step and converted into mixed oxides of Zn and Cd. Interestingly, some carbon atoms remained in the mixture that will be discussed in detail in XPS section.

The morphology and 2D microstructure of $\text{Zn}_{0.3}\text{Cd}_{0.7}\text{S}$ solid solution are shown via TEM images in Fig. 4. It is obvious that even after calcination and sulfuration steps, most of the microsphere structures were still preserved resulting from burning off carbon templates during calcination step (Fig. 4A, B). Clearly, these hollow spheres were mainly composed of well-defined nanoparticles of

$\text{Zn}_{0.3}\text{Cd}_{0.7}\text{S}$ solid solution in the range of 20 nm–100 nm (Fig. 4C–E). It should be mentioned that dispersing them in water for the photocatalytic reaction led to destroy the hollow structures. However, a high dispersion of nanoparticles was obtained throughout the solution that would help to generate considerable amount of hydrogen. Fig. 4F reveals the selected area electron diffraction (SAED) pattern of an individual particle of $\text{Zn}_{0.3}\text{Cd}_{0.7}\text{S}$ solid solution. The ring patterns can be attributed to (111), (220) and (311) planes with d -spacing of 0.32 nm, 0.19 nm, and 0.16 nm, respectively. Furthermore, high-resolution transmission electron microscope (HRTEM) perfectly shows the lattice structure of a typical nanoparticle. As it can be seen from Fig. 4H, the measurement shows that the interplanar spacing is 0.32 nm that corresponding to the interplanar distance of the (111) plane of $\text{Zn}_{0.3}\text{Cd}_{0.7}\text{S}$ [25].

Fig. 5 displays the nitrogen adsorption/desorption isotherms of the $\text{Zn}_x\text{Cd}_{1-x}\text{S}$ solid solutions at 77 K. All samples possessed a type IV isotherm and its adsorption capacity increased considerably with increasing the relative pressure (P/P_0 :0.9–1). The specific surface areas measured by the BET technique for all samples were around $15 \text{ m}^2 \text{ g}^{-1}$ (as shown in Table 1), which was mainly due to high temperature and ramp rate during calcination and sulfuration stages.

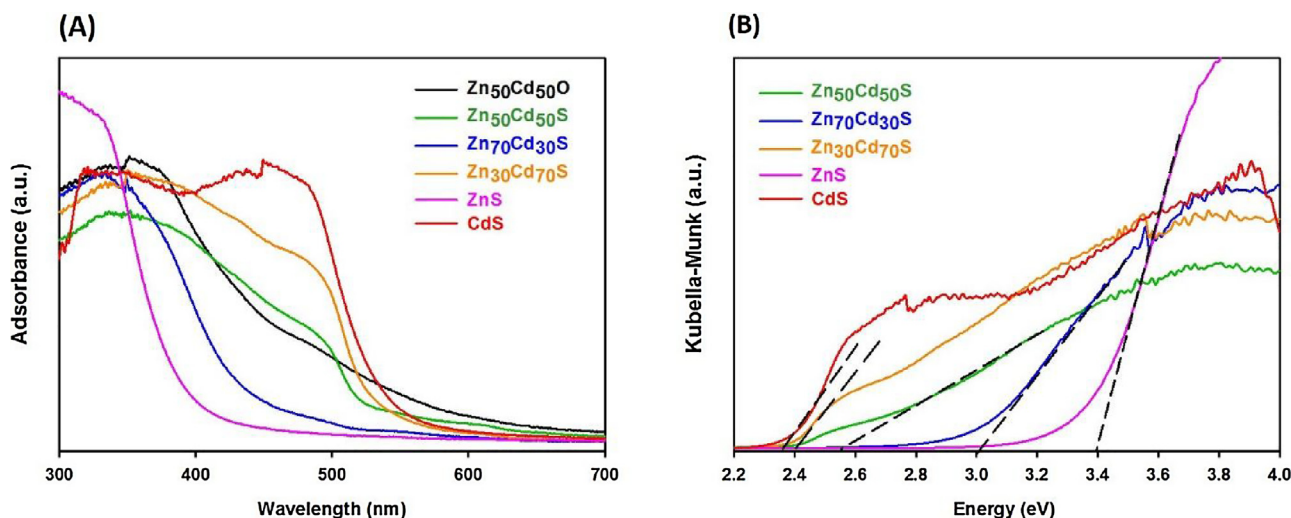


Fig. 2. UV-vis spectra and bandgap calculations of: $\text{Zn}_{0.50}\text{Cd}_{0.50}\text{O}$, $\text{Zn}_{0.5}\text{Cd}_{0.5}\text{S}$, $\text{Zn}_{0.7}\text{Cd}_{0.3}\text{O}$, $\text{Zn}_{0.3}\text{Cd}_{0.7}\text{O}$, ZnS and CdS .

According to representative XPS patterns in Fig. 6, Zn 2p showed two different peaks at 1044.9 and 1021.7 (eV) which are related to Zn 2p_{1/2} and Zn 2p_{3/2}, respectively. These binding energies confirmed that the valence state of zinc in the solid solution of $\text{Zn}_x\text{Cd}_{1-x}\text{S}$ and ZnS were the same. Furthermore, there are two various peaks of Cd which can be attributed to Cd 3d_{3/2} at 412.0 (eV) and Cd 3d_{5/2} at 405.2 (eV). In addition, the whole S 2p spectrum can be deconvoluted into two main peaks for S 2p_{1/2} and S 2p_{3/2} at 163.1 and 161.9 (eV), respectively. These binding energies of Zn, Cd and S are in good agreement with CdS and ZnS which are reported in the literature [13,14,32,33]. Interestingly, some carbon peaks were found in the XPS spectra of all samples. Although the samples were calcined at 500 °C for 4 h, some carbon residues were not able to react with oxygen and left the sample. The spectrum of C 1s can be deconvoluted into 3 main peaks of 285, 286.7 and 289 (eV), that can be related to C—C, C—O and C=O chemical bonds, respectively (Fig. 6D). The proportion of different elements in the XPS spectrum are calculated as follows: Zn: 16.08%, O 9.57%, Cd 35.23%, C 8.68%, S 30.45%. The EDS of different particles of $\text{Zn}_{0.3}\text{Cd}_{0.7}\text{S}$ solid solution also confirmed the same distribution of elements throughout the sample (Fig. 7).

Hydrogen production of $\text{Zn}_x\text{Cd}_{1-x}\text{S}$ in various conditions and different cocatalysts under solar simulator light with UV cut-off filter are displayed in Fig. 8. First, the optimum amount of Pt as a cocatalyst was found because its concentration play an important role in photocatalysis processes. Small amount of it cannot produce enough active sites for reduction reactions, although large amount of cocatalyst could lead to reduce light absorption on the photocatalyst surface which results in lower hydrogen generation. The highest hydrogen production rate of $\text{Zn}_x\text{Cd}_{1-x}\text{S}$ solid solution

was achieved by using 2 wt% of Pt. This optimum amount of cocatalyst was the same in various concentration of Zn and Cd. It should be mentioned that using a noble-metal-free cocatalyst has some privileges in comparison with platinum because of its low cost and wide availability. Interestingly, photo-deposition of MoS_2 as a cocatalyst on the surface of $\text{Zn}_x\text{Cd}_{1-x}\text{S}$ solid solution led to have the same hydrogen evolution rate under visible light illumination and its optimum amount was found to be 3 wt% (Fig. 8B). Moreover, MoS_2 can be synthesized and deposited on various semiconductors via different approaches that would lead to developing more practical and efficient photocatalysts [34–37].

The observed high activity of MoS_2 can be attributed to physical and electrochemical properties of molybdenum and MoS_2 . Firstly, Mo has smaller electronegativity than Pt (Pauling scale: 2.16 and 2.28, respectively) [38–41]. Moreover, MoS_2 is a semiconductor with a direct band gap of 1.68 eV, which consists of the conduction band of Mo metal and valence band of S species [41,42]. The small band gap of MoS_2 helps that the excited charge carriers have a longer lifetime before recombination with together. In addition, the similarity of valence bands of MoS_2 and $\text{Zn}_x\text{Cd}_{1-x}\text{S}$ leads to having the better-excited charge flow between the cocatalyst and the support. Furthermore, the work function of MoS_2 (5.15–5.39 eV) is slightly lower than Pt (5.22–5.60 eV) and so both cocatalysts showed similar performance for hydrogen generation [42–44]. Therefore, the mechanism of hydrogen production can be explained as follows. First, the $\text{Zn}_x\text{Cd}_{1-x}\text{S}$ solid solution absorbs the energy of light photons and produces excited electron and holes in its conduction and valence bands, respectively. Then, the excited electrons transfer to MoS_2 because of its conduction band position and over there they react with protons and produce hydrogen. A

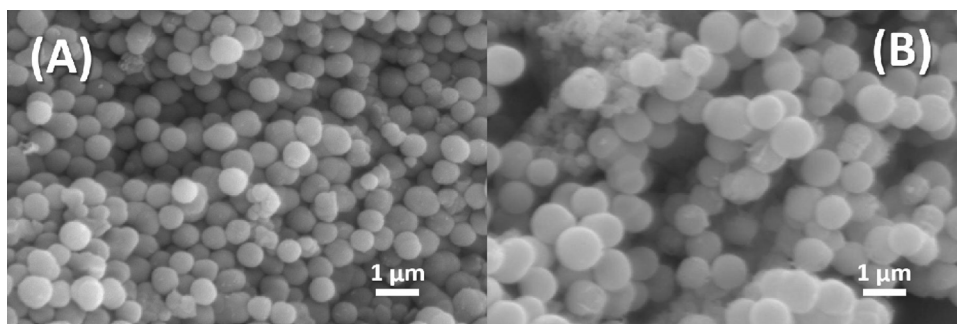


Fig. 3. SEM images of ZnCd -glycerate after synthesized in an autoclave.

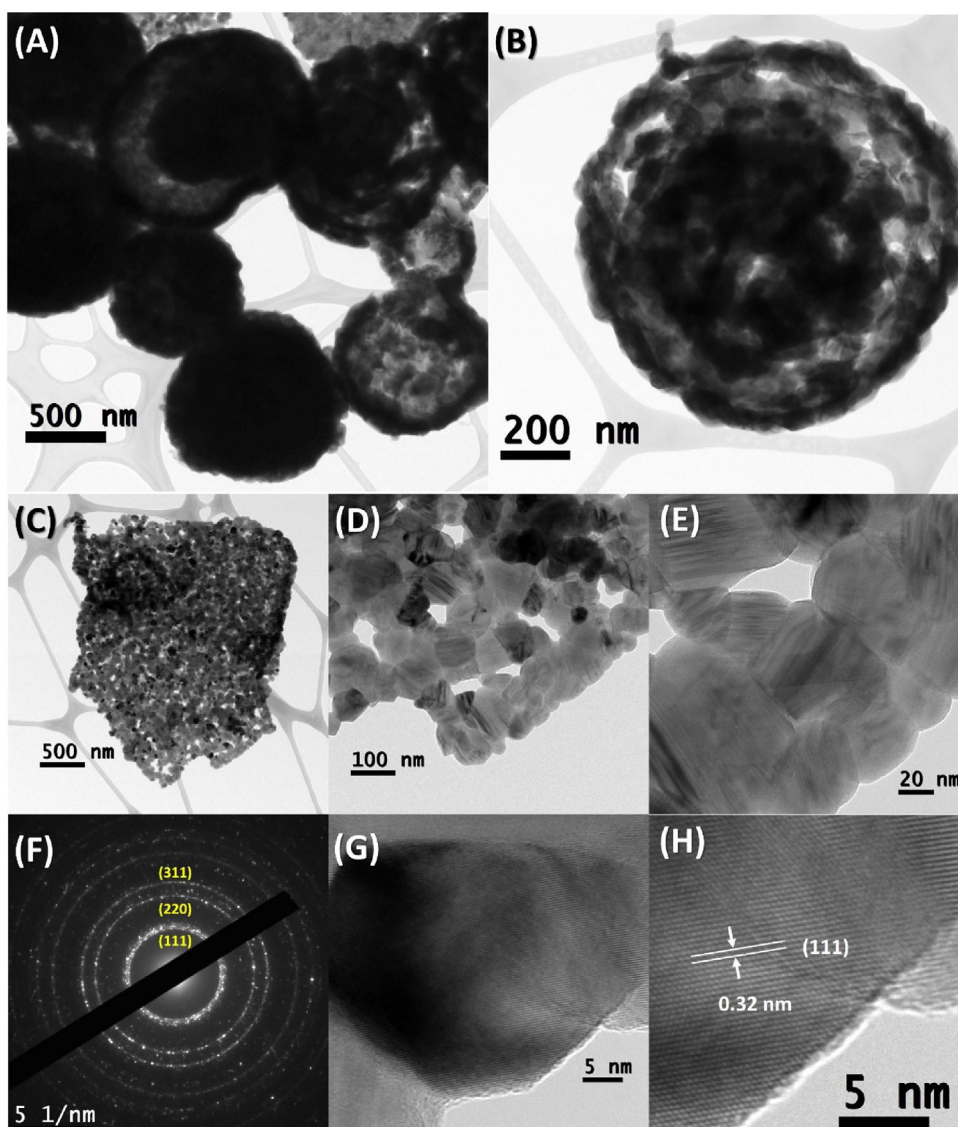


Fig. 4. (A–E) TEM images, (F) SAED pattern and (G,H) HRTEM of $\text{Zn}_{0.3}\text{Cd}_{0.7}\text{S}$ after H_2S treatment.

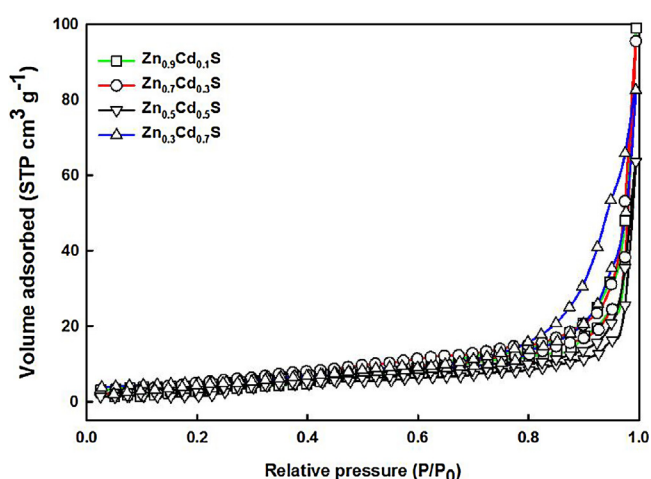


Fig. 5. Nitrogen adsorption–desorption isotherms at 77 K of $\text{Zn}_x\text{Cd}_{1-x}\text{S}$.

mixture of $\text{Na}_2\text{S}/\text{Na}_2\text{SO}_3$ was used as sacrificial reagent and their roles to provide sulfide ions can be explained as follows: Na_2S generates S^{2-} ions that is more unstable than sulfide photocatalyst; As a result, photoexcited holes oxidize Na_2S and produce polysulfide ions (S_n^{2-}); Then, the presence of SO_3^{2-} converts back the S_n^{2-} ions into S^{2-} [45].

Fig. 8C exhibits hydrogen generation of various concentration of $\text{Zn}_x\text{Cd}_{1-x}\text{S}$ solid solutions under full spectrum illumination of solar simulator after 3 h. Clearly, the highest amount of hydrogen produced with $\text{Zn}_{0.3}\text{Cd}_{0.7}\text{S}$ solid solution which was around $12.206 \text{ mmol h}^{-1} \text{ gr}^{-1}$. Moreover, this photocatalyst could produce more than $7.2 \text{ mmol h}^{-1} \text{ gr}^{-1}$ of hydrogen under visible light illumination ($\lambda \geq 420 \text{ nm}$). This amount of hydrogen generation was significantly higher than other concentrations of Zn and Cd. The reason could be attributed to the good

Table 1
Specific surface area measured by BET technique.

Sample	$\text{Zn}_{0.9}\text{Cd}_{0.1}\text{S}$	$\text{Zn}_{0.7}\text{Cd}_{0.3}\text{S}$	$\text{Zn}_{0.5}\text{Cd}_{0.5}\text{S}$	$\text{Zn}_{0.3}\text{Cd}_{0.7}\text{S}$
BET Surface Area ($\text{m}^2 \text{ g}^{-1}$)	12	17	15	16

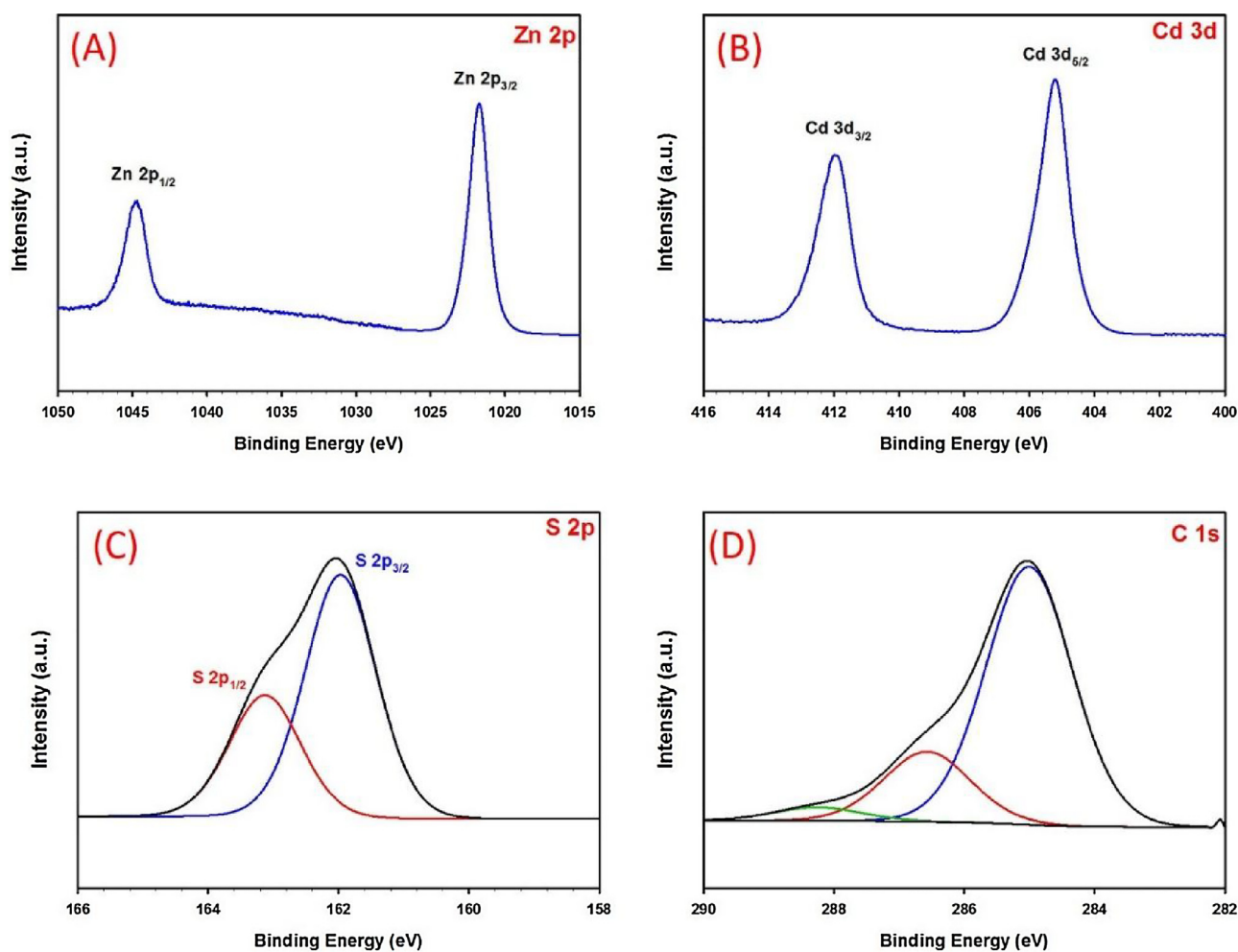


Fig. 6. XPS spectra of (A) Zn 2p, (B) Cd 3d, (C) S 2p and (D) C 1s of $\text{Zn}_{0.3}\text{Cd}_{0.7}\text{S}$.

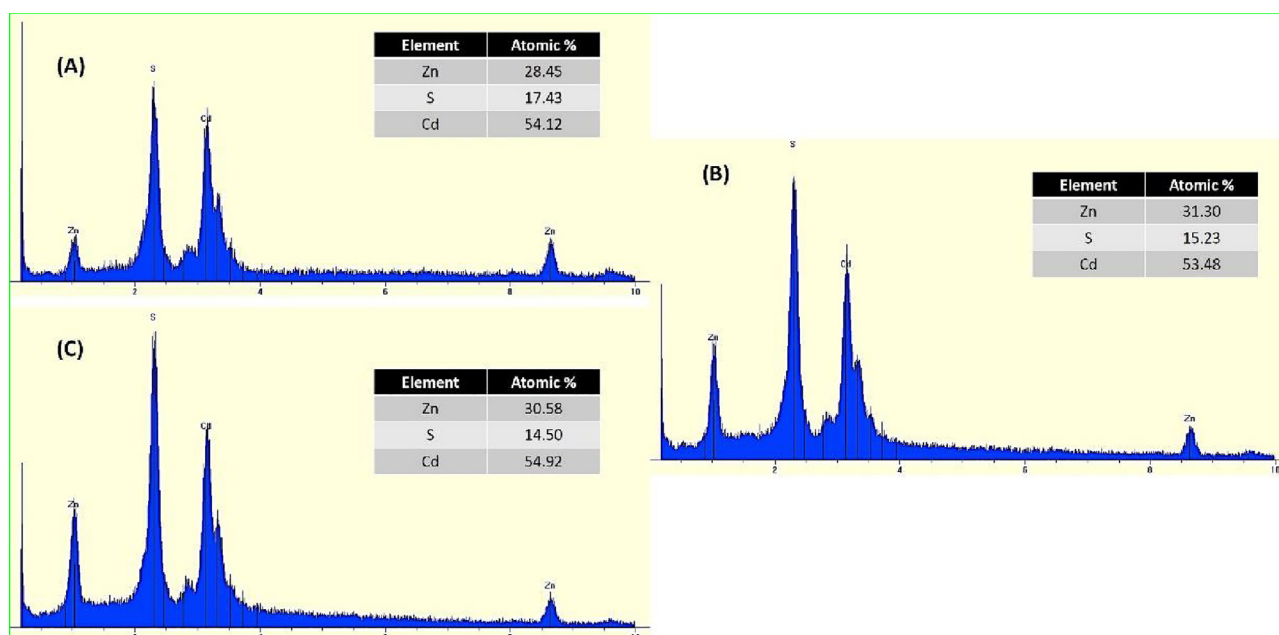


Fig. 7. EDS analysis of three different particles of $\text{Zn}_{0.3}\text{Cd}_{0.7}\text{S}$ solid solution.

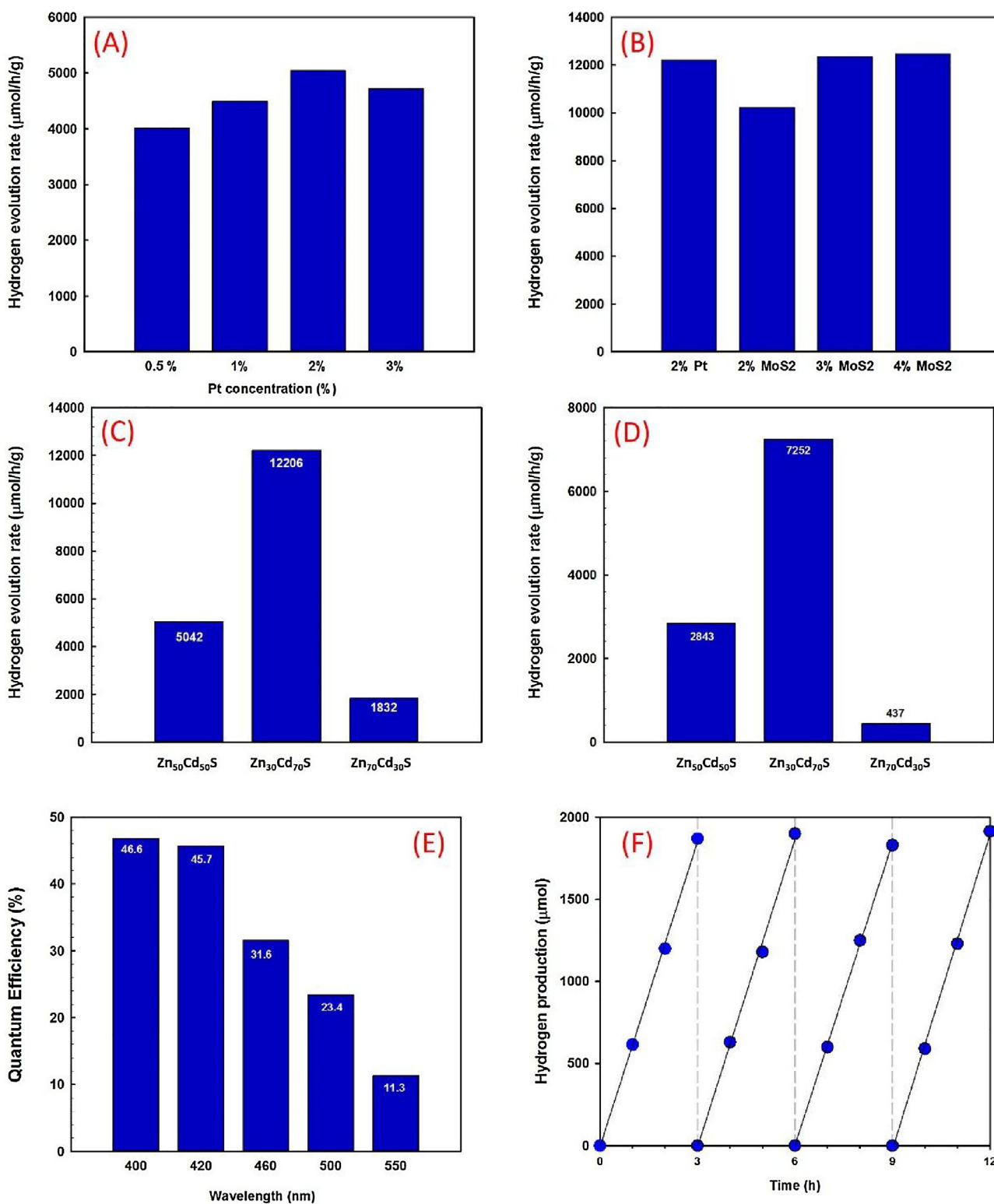


Fig. 8. Hydrogen production of (A) $\text{Zn}_x\text{Cd}_{1-x}\text{S}$ with various concentration of Pt as a cocatalyst under visible light ($\lambda > 420$ nm), (B) 2% of Pt and different concentration of MoS_2 as cocatalysts deposited via photodeposited on $\text{Zn}_{0.3}\text{Cd}_{0.7}\text{S}$ (full spectrum), (C) various concentration of Zn and Cd in a solid solution of $\text{Zn}_x\text{Cd}_{1-x}\text{S}$ under solar simulator full spectrum and (D) under visible light ($\lambda > 420$ nm) with 3% MoS_2 as a cocatalyst. (E) Quantum efficiency of $\text{Zn}_{0.3}\text{Cd}_{0.7}\text{S}$ in various wavelengths under solar simulator irradiations via 3% MoS_2 as a cocatalyst. (F) Hydrogen production of $\text{Zn}_{0.3}\text{Cd}_{0.7}\text{S}$ for 4 cycles. Reaction Conditions: 50 mg of photocatalyst was dispersed in 100 ml aqueous solution of 0.5 M Na_2S and Na_2SO_3 under simulator solar light 1:5 AM(ABET), equipped with 150 W Xe lamp.

development of crystal structure of Zn and Cd in this solid solution and narrower band gap of $\text{Zn}_{0.3}\text{Cd}_{0.7}\text{S}$ in comparison with other concentrations. Furthermore, the quantum efficiencies of the $\text{Zn}_{0.3}\text{Cd}_{0.7}\text{S}$ solid solution was calculated via the

various bandpass filters. Quantum efficiency at 400 and 420 nm are almost the same due to the fact that this semiconductor can mostly excited in visible light region (46.6% and 45.7%, respectively). Interestingly, this solid solution was even active

at longer wavelengths up to 550 nm with QE of 11.3%, as can be seen in Fig. 8E. Based on literatures, all QEs of $\text{Zn}_{0.3}\text{Cd}_{0.7}\text{S}$ with MoS_2 in various wavelengths, are among the highest QEs that has been reported for this kind of material [26]. Moreover, the hydrogen evolution of this photocatalyst was stable during different cycles as can be seen in Fig. 8F. It means that during photocatalytic reactions the excited holes and electrons react with protons and sacrificial reagents and no photocorrosion happened.

This such high activity of $\text{Zn}_{0.3}\text{Cd}_{0.7}\text{S}$ with MoS_2 as a cocatalyst in a wide range of visible light spectrum can be explained by the uniform creation of hexagonal solid solution of ZnS and CdS. Furthermore, oxygen replacement by S^{2-} during sulfuration step led to having some defects on the surface of the solid solution, which could be acted as photoexcited charges pools [24,46]. They not only help to deposit cocatalyst easier on the surface of the photocatalyst, but also cause to produce even more hydrogen.

4. Conclusion

The zinc cadmium sulfide ($\text{Zn}_x\text{Cd}_{1-x}\text{S}$) solid solution is one of the best semiconductors can act as a photocatalyst to generate hydrogen from water under sunlight illumination. Its crystal structure as a solid solution can be controlled by varying different amount of Zn/Cd ratio. Therefore, this solid solution possesses an adjustable conduction and valence bands positions as well as controllable band gap. In addition, its considerably stronger stability in comparison with CdS alone during photocatalytic reactions, make it a good candidate for the further industrial application. In this work, metal-glycerate from zinc and cadmium was synthesized via the solvothermal method. Then, the mixture of mixed oxides of ZnO and CdO was created from the metal-glycerate. After this step, sulfide ions (S^{2-}) was used in order to convert mixed oxides into solid solution of $\text{Zn}_x\text{Cd}_{1-x}\text{S}$. The obtained semiconductor can absorb a wide range of visible light energy because of its narrow band gap. The best results for hydrogen production from water splitting reaction were obtained by utilizing Zn/Cd = 0.3/0.7. Interestingly, utilizing MoS_2 as a cocatalyst could generate almost the same amount of hydrogen as Pt which was around $12 \text{ mmol h}^{-1} \text{ g}^{-1}$ hydrogen under solar simulator illumination. Moreover, the calculated quantum efficiencies were 46.6% at 400 nm, 23.4% at 500 nm and 11.3% at 550 nm, which were among the highest quantum efficiencies have ever reported for this semiconductor.

References

- [1] A. Fujishima, K. Honda, Electrochemical photolysis of water at a semiconductor electrode, *Nature* 238 (1972) 37–38.
- [2] N.S. Lewis, G. Crabtree, Basic Research Needs for Solar Energy Utilization: Report of the Basic Energy Sciences Workshop on Solar Energy Utilization, April 18–21 2005, US Department of Energy, Office of Basic Energy Science, 2005.
- [3] N.L. Panwar, S.C. Kaushik, S. Kothari, Role of renewable energy sources in environmental protection: a review, *Renew. Sustain. Energy Rev.* 15 (2011) 1513–1524.
- [4] M.R. Gholipour, C.-T. Dinh, F. Bédard, T.-O. Do, Nanocomposite heterojunctions as sunlight-driven photocatalysts for hydrogen production from water splitting, *Nanoscale* 7 (2015) 8187–8208.
- [5] X. Chen, S. Shen, L. Guo, S.S. Mao, Semiconductor-based photocatalytic hydrogen generation, *Chem. Rev.* 110 (2010) 6503–6570.
- [6] F. del Valle, A. Ishikawa, K. Domen, J.A. Villoria de la Mano, M.C. Sánchez-Sánchez, I.D. González, S. Herreras, N. Mota, M.E. Rivas, M.C. Álvarez Galván, J.L. G. Fierro, R.M. Navarro, Influence of Zn concentration in the activity of $\text{Cd}_{1-x}\text{Zn}_x\text{S}$ solid solutions for water splitting under visible light, *Catal. Today* 143 (2009) 51–56.
- [7] Y. Wang, J. Wu, J. Zheng, R. Xu, Highly active $\text{ZnxCd}_{1-x}\text{S}$ photocatalysts containing earth abundant elements only for H_2 production from water under visible light, *Catal. Sci. Technol.* 1 (2011) 940.
- [8] S. Ikeda, T. Nakamura, T. Harada, M. Matsumura, A. Kudo, H. Araki, A. Takeuchi, A. Holzinger, S. Jost, R. Hock, T. Vos, J. Schulze, A. Kirbs, Multicomponent sulfides

- as narrow gap hydrogen evolution photocatalysts, *Phys. Chem. Chem. Phys.* 12 (2010) 13943.
- [9] D. Meissner, R. Memming, B. Kastening, Photoelectrochemistry of cadmium sulfide. 1. Reanalysis of photocorrosion and flat-band potential, *J. Phys. Chem.* 92 (1988) 3476–3483.
- [10] U. Gaya, *Heterogeneous Photocatalysis Using Inorganic Semiconductor Solids*, 21, Springer Science & Business Media, 2013, pp. 213.
- [11] A. Kudo, Y. Miseki, Heterogeneous photocatalyst materials for water splitting, *Chem. Soc. Rev.* 38 (2009) 253–278.
- [12] C.-C. Chan, C.-C. Chang, C.-H. Hsu, Y.-C. Weng, K.-Y. Chen, H.-H. Lin, W.-C. Huang, S.-F. Cheng, Efficient and stable photocatalytic hydrogen production from water splitting over $\text{Zn}_x\text{Cd}_{1-x}\text{S}$ solid solutions under visible light irradiation, *Int. J. Hydrogen Energy* 39 (2014) 1630–1639.
- [13] Q. Li, H. Meng, P. Zhou, Y. Zheng, J. Wang, J. Yu, J. Gong, $\text{Zn}_{1-x}\text{Cd}_x\text{S}$ solid solutions with controlled bandgap and enhanced visible-light photocatalytic H_2 -production activity, *ACS Catal.* 3 (2013) 882.
- [14] Z. Mei, M. Zhang, J. Schneider, W. Wang, N. Zhang, Y. Su, B. Chen, S. Wang, A.L. Rogach, F. Pan, Hexagonal $\text{Zn}_{1-x}\text{Cd}_x\text{S}$ ($0.2 \leq x \leq 1$) solid solution photocatalysts for H_2 generation from water, *Catal. Sci. Technol.* (2017) 2–7.
- [15] C. Acar, I. Dincer, G.F. Naterer, Review of photocatalytic water-splitting methods for sustainable hydrogen production, *Int. J. Energy Res.* 40 (2016) 1449–1473.
- [16] K. Maeda, K. Domen, Photocatalytic water splitting: recent progress and future challenges, *J. Phys. Chem. Lett.* 1 (2010) 2655–2661.
- [17] T. Hisatomi, K. Takahashi, K. Domen, Photocatalytic water-splitting reaction from catalytic and kinetic perspectives, *Catal. Lett.* 145 (2014) 95–108.
- [18] C. Xing, Y.W. Zhang Yan, L. Guo, Band structure-controlled solid solution of $\text{Cd}_{1-x}\text{Zn}_x\text{S}$ photocatalyst for hydrogen production by water splitting, *Int. J. Hydrogen Energy* 31 (2006) 2018–2024.
- [19] K. Zhang, D. Jing, C. Xing, L. Guo, Significantly improved photocatalytic hydrogen production activity over $\text{Cd}_{1-x}\text{Zn}_x\text{S}$ photocatalysts prepared by a novel thermal sulfuration method, *Int. J. Hydrogen Energy* 32 (2007) 4685–4691.
- [20] G. Liu, L. Zhao, L. Ma, L. Guo, Photocatalytic H_2 evolution under visible light irradiation on a novel $\text{Cd}_x\text{Cu}_y\text{Zn}_{1-x-y}\text{S}$ catalyst, *Catal. Commun.* 9 (2008) 126–130.
- [21] D. Zhang, M. Liu, L. Guo, Efficient photocatalytic H_2 production under visible light irradiation over Ni doped $\text{Cd}_{1-x}\text{Zn}_x\text{S}$ microsphere photocatalysts, *Catal. Commun.* 9 (2008) 1720–1724.
- [22] G. Liu, Z. Zhou, L. Guo, Correlation between band structures and photocatalytic activities of $\text{Cd}_x\text{Cu}_y\text{Zn}_{1-x-y}\text{S}$ solid solution, *Chem. Phys. Lett.* 509 (2011) 43–47.
- [23] X. Wang, G. Liu, Z.-G. Chen, F. Li, G.Q. (Max) Lu, H.-M. Cheng, Efficient and stable photocatalytic H_2 evolution from water splitting by ($\text{Cd}_0.8\text{Zn}_0.2$)S nanorods, *Electrochem. Commun.* 11 (2009) 1174–1178.
- [24] J. Shi, H. n. Cui, Z. Liang, X. Lu, Y. Tong, C. Su, H. Liu, The roles of defect states in photoelectric and photocatalytic processes for $\text{ZnxCd}_{1-x}\text{S}$, *Energy Environ. Sci.* 4 (2011) 466.
- [25] L. Wang, W. Wang, M. Shang, W. Yin, S. Sun, L. Zhang, Enhanced photocatalytic hydrogen evolution under visible light over $\text{Cd}_{1-x}\text{Zn}_x\text{S}$ solid solution with cubic zinc blend phase, *Int. J. Hydrogen Energy* 35 (2010) 19–25.
- [26] M. Liu, Y. Chen, J. Su, J. Shi, X. Wang, L. Guo, Photocatalytic hydrogen production using twinned nanocrystals and an unanchored NiSx co-catalyst, *Nat. Energy* 1 (2016) 16151.
- [27] C.-C. Shen, Y.-N. Liu, X. Zhou, H.-L. Guo, Z.-W. Zhao, K. Liang, A.-W. Xu, Large improvement of visible-light photocatalytic H_2 -evolution based on cocatalyst-free $\text{Zn}_{0.5}\text{Cd}_{0.5}\text{S}$ synthesized through a two-step process, *Catal. Sci. Technol.* 7 (2017) 961–967.
- [28] M. Liu, L. Wang, G. (Max) Lu, X. Yao, L. Guo, D. Arcon, S. Herreras, N. Mota, M.E. Rivas, M.C.A. Galvan, J.L.G. Fierro, R.M. Navarro, Twins in $\text{Cd}_{1-x}\text{Zn}_x\text{S}$ solid solution: highly efficient photocatalyst for hydrogen generation from water, *Energy Environ. Sci.* 4 (2011) 1372.
- [29] L. Shen, L. Yu, H.B. Wu, X.-Y. Yu, X. Zhang, X.W.D. Lou, Formation of nickel cobalt sulfide ball-in-ball hollow spheres with enhanced electrochemical pseudocapacitive properties, *Nat. Commun.* 6 (2015) 6694.
- [30] L. Shen, L. Yu, X.-Y. Yu, X. Zhang, X.W.D. Lou, Self-templated formation of uniform NiCo_2O_4 hollow spheres with complex interior structures for lithium-ion batteries and supercapacitors, *Angew. Chem. Int. Ed.* 54 (2015) 1868–1872.
- [31] K. Shimura, H. Yoshida, Heterogeneous photocatalytic hydrogen production from water and biomass derivatives, *Energy Environ. Sci.* 4 (2011) 2467.
- [32] M. Tejos R, B.G. Rolón, R. Del Río, G. Cabello, Investigation and optical evaluation of precursors for the photodeposition of nanosized ZnS amorphous thin films, *J. Chil. Chem. Soc.* 52 (2007) 1257–1260.
- [33] L. Qi, J. Yu, M. Jaroniec, Preparation and enhanced visible-light photocatalytic H_2 -production activity of CdS-sensitized Pt/TiO₂ nanosheets with exposed (001) facets, *Phys. Chem. Chem. Phys.* 13 (2011) 8915–8923.
- [34] U. Maitra, U. Gupta, M. De, R. Datta, A. Govindaraj, C. Rao, Highly effective visible-light-induced H_2 generation by single-layer 1T-MoS₂ and a nanocomposite of few-layer 2H-MoS₂ with heavily nitrogenated graphene, *Angew. Chem. Int. Ed.* 52 (2013) 13057–13061.
- [35] Y. Li, H. Wang, S. Peng, Tunable photodeposition of MoS₂ onto a composite of reduced graphene oxide and CdS for synergic photocatalytic hydrogen generation, *J. Phys. Chem. C* 118 (2014) 19842–19848.
- [36] Y. Lu, D. Wang, P. Yang, Y. Du, C. Lu, Coupling $\text{ZnxCd}_{1-x}\text{S}$ nanoparticles with graphene-like MoS₂: superior interfacial contact, low overpotential and enhanced photocatalytic activity under visible-light irradiation, *Catal. Sci. Technol.* 4 (2014) 2650–2657.

- [37] Z. Wang, J. Hou, C. Yang, S. Jiao, H. Zhu, Three-dimensional MoS₂-CdS-[gamma]-TaON hollow composites for enhanced visible-light-driven hydrogen evolution, *Chem. Commun.* 50 (2014) 1731–1734.
- [38] A.D. McNaught, A. Wilkinson, I.U.o.P.a.A. Chemistry. Compendium of Chemical Terminology: IUPAC Recommendations, (1997) .
- [39] V. Gold, I.U.o.P.a.A. Chemistry. Compendium of Chemical Terminology: IUPAC Recommendations, (1987) , pp. 456.
- [40] L. Pauling, The nature of the chemical bond and the structure of molecules and crystals: an introduction to modern structural chemistry, *J. Am. Chem. Soc.* 82 (1960) 4121.
- [41] R.M. Irfan, D. Jiang, Z. Sun, L. Zhang, S. Cui, P. Du, Incorporating a molecular co-catalyst with a heterogeneous semiconductor heterojunction photocatalyst: novel mechanism with two electron-transfer pathways for enhanced solar hydrogen production, *J. Catal.* 353 (2017) 274–285.
- [42] H. Zhong, Z. Ni, Y. Wang, M. Ye, Z. Song, Y. Pan, R. Quhe, J. Yang, L. Yang, J. Shi, J. Lu, Interfacial properties of monolayer and bilayer MoS₂ contacts with metals: beyond the energy band calculations, *Sci. Rep* 6 (2015) 21786.
- [43] S. Choi, Z. Shaolin, W. Yang, Layer-number-dependent work function of MoS₂ nanoflakes, *J. Korean Phys. Soc.* 64 (2014) 1550–1555.
- [44] D. Dai, H. Xu, L. Ge, C. Han, Y. Gao, S. Li, Y. Lu, In-situ synthesis of CoP co-catalyst decorated Zn_{0.5}Cd_{0.5}S photocatalysts with enhanced photocatalytic hydrogen production activity under visible light irradiation, *Appl. Catal. B* 217 (2017) 429–436.
- [45] M. Wang, S. Shen, L. Li, Z. Tang, J. Yang, Effects of sacrificial reagents on photocatalytic hydrogen evolution over different photocatalysts, *J. Mater. Sci.* 52 (2017) 5155–5164.
- [46] R. Chen, K. Li, X.-S. Zhu, S.-L. Xie, L.-Z. Dong, S.-L. Li, Y.-Q. Lan, In situ synthesis of porous ZnO-embedded Zn_{1-x}Cd_xS/CdS heterostructures for enhanced photocatalytic activity, *CrystEngComm* 18 (2016) 1446–1452.